Minijet deformation and charge-independent two-particle correlations on momentum subspace (η, ϕ) in Au-Au collisions at $\sqrt{s_{NN}} = 130$ GeV

J. Adams,[3] M.M. Aggarwal,[29] Z. Ahammed,[43] J. Amonett,[20] B.D. Anderson,[20] D. Arkhipkin,[13] G.S. Averichev,[12] S.K. Badyal,[19] Y. Bai,[27] J. Balewski,[17] O. Barannikova,[32] L.S. Barnby,[3] J. Baudot,[18] S. Bekele,[28] V.V. Belaga,[12] R. Bellwied,[46] J. Berger,[14] B.I. Bezverkhny,[48] S. Bharadwaj,[33] A. Bhasin,[19] A.K. Bhati,[29] V.S. Bhatia,[29] H. Bichsel,[45] A. Billmeier,[46] L.C. Bland,[4] C.O. Blyth,[3] B.E. Bonner,[34] M. Botje,[27] A. Boucham,[38] A.V. Brandin,[25] A. Bravar,[4] M. Bystersky,[11] R.V. Cadman,[1] X.Z. Cai,[37] H. Caines,[48] M. Calderón de la Barca Sánchez,[4] J. Carroll,[21] J. Castillo,[21] D. Cebra,[7] Z. Chajecki,[44] P. Chaloupka,[11] S. Chattopdhyay,[43] H.F. Chen,[36] Y. Chen,[8] J. Cheng,[41] M. Cherney,[10] A. Chikanian,[48] W. Christie,[4] J.P. Coffin,[18] T.M. Cormier,[46] J.G. Cramer,[45] H.J. Crawford,[6] D. Das,[43] S. Das,[43] M.M. de Moura,[35] A.A. Derevschikov,[31] L. Didenko,[4] T. Dietel,[14] S.M. Dogra,[19] W.J. Dong,[8] X. Dong,[36] J.E. Draper,[7] F. Du,[48] A.K. Dubey,[15] V.B. Dunin,[12] J.C. Dunlop,[4] M.R. Dutta Mazumdar,[43] V. Eckardt,[23] W.R. Edwards,[21] L.G. Efimov,[12] V. Emelianov,[25] J. Engelage,[6] G. Eppley,[34] B. Erazmus,[38] M. Estienne,[38] P. Fachini,[4] J. Faivre,[18] R. Fatemi,[17] J. Fedorisin,[12] K. Filimonov,[21] P. Filip,[11] E. Finch,[48] V. Fine,[4] Y. Fisyak,[4] K.J. Foley,[4] K. Fomenko,[12] J. Fu,[41] C.A. Gagliardi,[39] J. Gans,[48] M.S. Ganti,[43] L. Gaudichet,[38] F. Geurts,[34] V. Ghazikhanian,[8] P. Ghosh,[43] J.E. Gonzalez,[8] O. Grachov,[46] O. Grebenyuk,[27] D. Grosnick,[42] S.M. Guertin,[8] Y. Guo,[46] A. Gupta,[19] T.D. Gutierrez,[7] T.J. Hallman,[4] A. Hamed,[46] D. Hardtke,[21] J.W. Harris,[48] M. Heinz,[2] T.W. Henry,[39] S. Hepplemann,[30] B. Hippolyte,[48] A. Hirsch,[32] E. Hjort,[21] G.W. Hoffmann,[40] H.Z. Huang,[8] S.L. Huang,[36] E.W. Hughes,[5] T.J. Humanic,[28] G. Igo,[8] A. Ishihara,[40] P. Jacobs,[21] W.W. Jacobs,[17] M. Janik,[44] H. Jiang,[8] P.G. Jones,[3] E.G. Judd,[6] S. Kabana,[2] K. Kang,[41] M. Kaplan,[9] D. Keane,[20] V.Yu. Khodyrev,[31] J. Kiryluk,[22] A. Kisiel,[44] E.M. Kislov,[12] J. Klay,[21] S.R. Klein,[21] A. Klyachko,[17] D.D. Koetke,[42] T. Kollegger,[14] M. Kopytine,[20] L. Kotchenda,[25] M. Kramer,[26] P. Kravtsov,[25] V.I. Kravtsov,[31] K. Krueger,[1] C. Kuhn,[18] A.I. Kulikov,[12] A. Kumar,[29] C.L. Kunz,[9] R.Kh. Kutuev,[13] A.A. Kuznetsov,[12] M.A.C. Lamont,[48] J.M. Landgraf,[4] S. Lange,[14] F. Laue,[4] J. Lauret,[4] A. Lebedev,[4] R. Lednicky,[12] S. Lehocka,[12] M.J. LeVine,[4] C. Li,[36] Q. Li,[46] Y. Li,[41] S.J. Lindenbaum,[26] M.A. Lisa,[28] F. Liu,[47] L. Liu,[47] Q.J. Liu,[45] Z. Liu,[47] T. Ljubicic,[4] W.J. Llope,[34] H. Long,[8] R.S. Longacre,[4] M. Lopez-Noriega,[28] W.A. Love,[4] Y. Lu,[47] T. Ludlam,[4] D. Lynn,[4] G.L. Ma,[37] J.G. Ma,[8] Y.G. Ma,[37] D. Magestro,[28] S. Mahajan,[19] D.P. Mahapatra,[15] R. Majka,[48] L.K. Mangotra,[19] R. Manweiler,[42] S. Margetis,[20] C. Markert,[48] L. Martin,[38] J.N. Marx,[21] H.S. Matis,[21] Yu.A. Matulenko,[31] C.J. McClain,[1] T.S. McShane,[10] F. Meissner,[21] Yu. Melnick,[31] A. Meschanin,[31] M.L. Miller,[22] Z. Milosevich,[9] N.G. Minaev,[31] C. Mironov,[20] A. Mischke,[27] D.K. Mishra,[15] J. Mitchell,[34] B. Mohanty,[43] L. Molnar,[32] C.F. Moore,[40] D.A. Morozov,[31] M.G. Munhoz,[35] B.K. Nandi,[43] S.K. Nayak,[19] T.K. Nayak,[43] J.M. Nelson,[3] P.K. Netrakanti,[43] V.A. Nikitin,[13] L.V. Nogach,[31] S.B. Nurushev,[31] G. Odyniec,[21] A. Ogawa,[4] V. Okorokov,[25] M. Oldenburg,[21] D. Olson,[21] S.K. Pal,[43] Y. Panebratsev,[12] S.Y. Panitkin,[4] A.I. Pavlinov,[46] T. Pawlak,[44] T. Peitzmann,[27] V. Perevoztchikov,[4] C. Perkins,[6] W. Peryt,[44] V.A. Petrov,[13] S.C. Phatak,[15] R. Picha,[7] M. Planinic,[49] J. Pluta,[44] N. Porile,[32] J. Porter,[45] A.M. Poskanzer,[21] M. Potekhin,[4] E. Potrebenikova,[12] B.V.K.S. Potukuchi,[19] D. Prindle,[45] C. Pruneau,[46] J. Putschke,[23] G. Rai,[21] G. Rakness,[30] R. Raniwala,[33] S. Raniwala,[33] O. Ravel,[38] R.L. Ray,[40] S.V. Razin,[12] D. Reichhold,[32] J.G. Reid,[45] G. Renault,[38] F. Retiere,[21] A. Ridiger,[25] H.G. Ritter,[21] J.B. Roberts,[34] O.V. Rogachevskiy,[12] J.L. Romero,[7] A. Rose,[46] C. Roy,[38] L. Ruan,[36] R. Sahoo,[15] I. Sakrejda,[21] S. Salur,[48] J. Sandweiss,[48] I. Savin,[13] P.S. Sazhin,[12] J. Schambach,[40] R.P. Scharenberg,[32] N. Schmitz,[23] L.S. Schroeder,[21] K. Schweda,[21] J. Seger,[10] P. Seyboth,[23] E. Shahaliev,[12] M. Shao,[36] W. Shao,[5] M. Sharma,[29] W.Q. Shen,[37] K.E. Shestermanov,[31] S.S. Shimanskiy,[12] E Sichtermann,[21] F. Simon,[23] R.N. Singaraju,[43] G. Skoro,[12] N. Smirnov,[48] R. Snellings,[27] G. Sood,[42] P. Sorensen,[21] J. Sowinski,[17] J. Speltz,[18] H.M. Spinka,[1] B. Srivastava,[32] A. Stadnik,[12] T.D.S. Stanislaus,[42] R. Stock,[14] A. Stolpovsky,[46] M. Strikhanov,[25] B. Stringfellow,[32] A.A.P. Suaide,[35] E. Sugarbaker,[28] C. Suire,[4] M. Sumbera,[11] B. Surrow,[22] T.J.M. Symons,[21] A. Szanto de Toledo,[35] P. Szarwas,[44] A. Tai,[8] J. Takahashi,[35] A.H. Tang,[27] T. Tarnowsky,[32] D. Thein,[8] J.H. Thomas,[21] S. Timoshenko,[25] M. Tokarev,[12] T.A. Trainor,[45] S. Trentalange,[8] R.E. Tribble,[39] O.D. Tsai,[8] J. Ulery,[32] T. Ullrich,[4] D.G. Underwood,[1] A. Urkinbaev,[12] G. Van Buren,[4] M. van Leeuwen,[21] A.M. Vander Molen,[24] R. Varma,[16] I.M. Vasilevski,[13] A.N. Vasiliev,[31] R. Vernet,[18] S.E. Vigdor,[17] Y.P. Viyogi,[43] S. Vokal,[12] S.A. Voloshin,[46] M. Vznuzdaev,[25] W.T. Waggoner,[10] F. Wang,[32] G. Wang,[20] G. Wang,[5] X.L. Wang,[36] Y. Wang,[40] Y. Wang,[41] Z.M. Wang,[36] H. Ward,[40] J.W. Watson,[20] J.C. Webb,[17] R. Wells,[28] G.D. Westfall,[24] A. Wetzler,[21] C. Whitten Jr.,[8] H. Wieman,[21] S.W. Wissink,[17] R. Witt,[2] J. Wood,[8] J. Wu,[36] N. Xu,[21] Z. Xu,[4] Z.Z. Xu,[36] E. Yamamoto,[21] P. Yepes,[34] V.I. Yurevich,[12] Y.V. Zanevsky,[12] H. Zhang,[4] W.M. Zhang,[20] Z.P. Zhang,[36] P.A Zolnierczuk,[17] R. Zoulkarneev,[13] Y. Zoulkarneeva,[13] and A.N. Zubarev[12]

(STAR Collaboration)

[1] *Argonne National Laboratory, Argonne, Illinois 60439*
[2] *University of Bern, 3012 Bern, Switzerland*
[3] *University of Birmingham, Birmingham, United Kingdom*
[4] *Brookhaven National Laboratory, Upton, New York 11973*
[5] *California Institute of Technology, Pasedena, California 91125*
[6] *University of California, Berkeley, California 94720*
[7] *University of California, Davis, California 95616*
[8] *University of California, Los Angeles, California 90095*
[9] *Carnegie Mellon University, Pittsburgh, Pennsylvania 15213*
[10] *Creighton University, Omaha, Nebraska 68178*
[11] *Nuclear Physics Institute AS CR, 250 68 Řež/Prague, Czech Republic*
[12] *Laboratory for High Energy (JINR), Dubna, Russia*
[13] *Particle Physics Laboratory (JINR), Dubna, Russia*
[14] *University of Frankfurt, Frankfurt, Germany*
[15] *Insitute of Physics, Bhubaneswar 751005, India*
[16] *Indian Institute of Technology, Mumbai, India*
[17] *Indiana University, Bloomington, Indiana 47408*
[18] *Institut de Recherches Subatomiques, Strasbourg, France*
[19] *University of Jammu, Jammu 180001, India*
[20] *Kent State University, Kent, Ohio 44242*
[21] *Lawrence Berkeley National Laboratory, Berkeley, California 94720*
[22] *Massachusetts Institute of Technology, Cambridge, MA 02139-4307*
[23] *Max-Planck-Institut für Physik, Munich, Germany*
[24] *Michigan State University, East Lansing, Michigan 48824*
[25] *Moscow Engineering Physics Institute, Moscow Russia*
[26] *City College of New York, New York City, New York 10031*
[27] *NIKHEF, Amsterdam, The Netherlands*
[28] *Ohio State University, Columbus, Ohio 43210*
[29] *Panjab University, Chandigarh 160014, India*
[30] *Pennsylvania State University, University Park, Pennsylvania 16802*
[31] *Institute of High Energy Physics, Protvino, Russia*
[32] *Purdue University, West Lafayette, Indiana 47907*
[33] *University of Rajasthan, Jaipur 302004, India*
[34] *Rice University, Houston, Texas 77251*
[35] *Universidade de Sao Paulo, Sao Paulo, Brazil*
[36] *University of Science & Technology of China, Anhui 230027, China*
[37] *Shanghai Institute of Applied Physics, Shanghai 201800, China*
[38] *SUBATECH, Nantes, France*
[39] *Texas A&M University, College Station, Texas 77843*
[40] *University of Texas, Austin, Texas 78712*
[41] *Tsinghua University, Beijing 100084, China*
[42] *Valparaiso University, Valparaiso, Indiana 46383*
[43] *Variable Energy Cyclotron Centre, Kolkata 700064, India*
[44] *Warsaw University of Technology, Warsaw, Poland*
[45] *University of Washington, Seattle, Washington 98195*
[46] *Wayne State University, Detroit, Michigan 48201*
[47] *Institute of Particle Physics, CCNU (HZNU), Wuhan 430079, China*
[48] *Yale University, New Haven, Connecticut 06520*
[49] *University of Zagreb, Zagreb, HR-10002, Croatia*

(Dated: November 4, 2004)

We present first measurements of charge-independent correlations on momentum-space difference variables $\eta_1 - \eta_2$ (pseudorapidity) and $\phi_1 - \phi_2$ (azimuth) for charged primary hadrons with transverse momentum within $0.15 \leq p_t \leq 2$ GeV/c and $|\eta| \leq 1.3$ from Au-Au collisions at $\sqrt{s_{NN}} = 130$ GeV. We observe strong charge-indepedendent correlations associated with minijets and elliptic flow. The width of the minijet peak on $\eta_1 - \eta_2$ increases by a factor 2.3 from peripheral to central collisions, suggesting strong coupling of partons to a longitudinally-expanding colored medium. New methods of jet analysis introduced here reveal nonperturbative medium effects in heavy ion collisions.

PACS numbers: 24.60.-k, 24.60.Ky, 25.75.Gz

Correlations and fluctuations access properties of the colored medium produced in ultrarelativistic heavy ion

collisions at RHIC [1, 2, 3]. *In-medium modification* of string fragmentation and hard parton scattering in heavy ion collisions should affect large-momentum-scale correlations ($|\phi_1-\phi_2| \sim \pi/2$, $|\eta_1-\eta_2| \sim 1$). Charge-independent correlations are produced by initial-state multiple scattering (Cronin effect [4], minijet production [5]) and in-medium dissipation [6]. Previous studies of parton-medium interactions included angular correlations of high-p_t particles (*e.g.,* leading-particle $p_t > 4$ GeV/c) in which the away-side jet structure was strongly reduced in central Au-Au collisions [7]. Theoretical descriptions of parton energy loss and medium-modified fragmentation include, respectively, pQCD-based jet-quenching models [5, 8] and parton recombination models [9].

In this Letter we report the first measurements in heavy ion collisions of charge-independent *joint autocorrelations* [10] on difference variables $\phi_\Delta \equiv \phi_1 - \phi_2$ (azimuth) *and* $\eta_\Delta \equiv \eta_1 - \eta_2$ (pseudorapidity) for charged particles with $0.15 \leq p_t \leq 2$ GeV/c. The observed correlation structure is dominated by minijets and elliptic flow. These *low-p_t* measurements of jet correlations suggest that in central collisions strong coupling of partons to a *longitudinally-expanding medium* [11] produces dramatic changes in the angular distributions of parton fragments not anticipated by theoretical models [5, 12]. This analysis is based on $\sqrt{s_{NN}} = 130$ GeV Au-Au collisions observed with the STAR detector at the Relativistic Heavy Ion Collider (RHIC).

The charge-independent (CI - all charged particles) autocorrelations obtained in this study access the complete structure of two-particle density $\rho(\vec{p_1}, \vec{p_2})$ projected onto momentum-space variables $(\eta_1, \eta_2, \phi_1, \phi_2)$. Differential analysis is achieved by comparing distributions of particle pairs taken from single events (sibling pairs) with particles paired from different but similar events (mixed pairs). The corresponding correlation function and ratio distribution are defined by

$$\begin{aligned} C(\vec{p}_1, \vec{p}_2) &= \rho_{mix}(\vec{p}_1, \vec{p}_2)\,[r(\vec{p}_1, \vec{p}_2) - 1]\,, \\ r(\vec{p}_1, \vec{p}_2) &= \rho_{sib}(\vec{p}_1, \vec{p}_2)/\rho_{mix}(\vec{p}_1, \vec{p}_2). \end{aligned} \quad (1)$$

Pair densities $\rho(\vec{p}_1, \vec{p}_2)$ are projected onto variable pairs (η_1, η_2), (ϕ_1, ϕ_2) and $(\eta_\Delta, \phi_\Delta)$ as histograms $n_{ij} \simeq \epsilon_x\, \epsilon_y\, \rho(x_i, y_j)$, where ϵ_x, ϵ_y are bin widths on $x, y \in \{\eta, \phi, \eta_\Delta, \phi_\Delta\}$. Sibling- and mixed-pair histograms are separately normalized to the total number of detected pairs in each event class: $\hat{n}_{ij} = n_{ij}/\sum_{ij} n_{ij}$. Normalized ratios $\hat{r}_{ij} = \hat{n}_{ij,sib}/\hat{n}_{ij,mix}$ are the basis for this analysis.

Data for this analysis were obtained with the STAR detector [13] using a 0.25 T uniform magnetic field parallel to the beam axis. Event triggering and charged-particle measurements with the time projection chamber (TPC) are described in [13]. Track definitions, tracking efficiencies, quality cuts and primary-particle definition are described in [14, 15]. Tracks were accepted in $|\eta| \leq 1.3$, $0.15 \leq p_t \leq 2$ GeV/c and full azimuth. Particle identification was not implemented. Corrections were made to $\hat{r}$ for two-track inefficiencies due to track merging and splitting [16]. Small-scale momentum correlations (SSC) due to HBT and Coulomb effects [17] were suppressed by eliminating track pairs with $|\eta_\Delta| < 0.3$, $|\phi_\Delta| < \pi/6$, $|p_{t1} - p_{t2}| < 0.15$ GeV/c, if $p_t < 0.8$ GeV/c for either particle. Ratios were formed from subsets of events with similar centrality (multiplicity differs by ≤ 50) and primary-vertex location (within 7.5 cm along beam axis) and combined as weighted averages within each centrality class. Four centrality classes (labeled (a) - (d) from central to peripheral) were defined [18] by cuts on track multiplicity N within the acceptance, relative to endpoint N_0 [19].

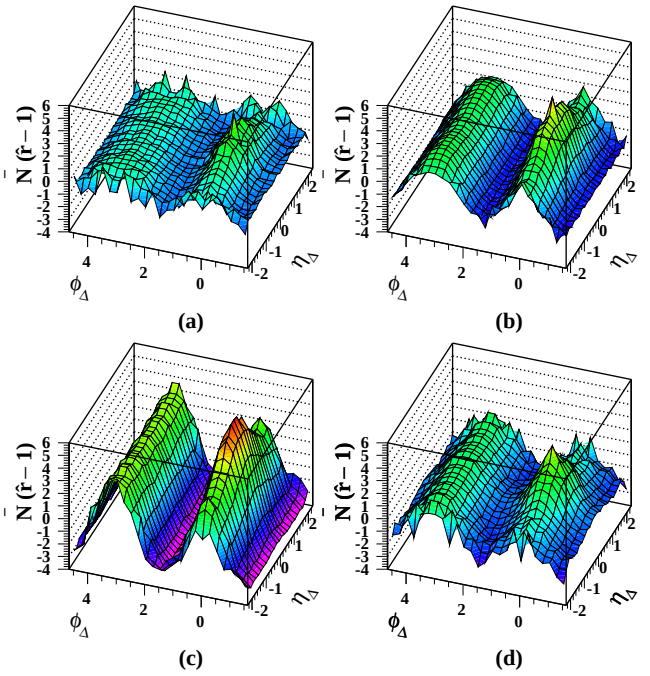

FIG. 1: Perspective views of two-particle CI joint autocorrelations $\bar{N}(\hat{r} - 1)$ on $(\eta_\Delta, \phi_\Delta)$ for central (a) to peripheral (d) collisions.

If correlation structure is invariant on sum variables $\eta_1 + \eta_2$ and $\phi_1 + \phi_2$, as in these heavy ion collisions [20], distributions $\hat{r}$ can be projected along those sum variables to form 1D autocorrelations on corresponding difference variables *without information loss.* 2D *joint* autocorrelations on difference variables $(\eta_\Delta, \phi_\Delta)$ then compactly represent all correlations on momentum subspace $(\eta_1, \eta_2, \phi_1, \phi_2)$ using only two variables. Plotted in Fig. 1 are perspective views of CI joint autocorrelations $\bar{N}(\hat{r}-1)$ (measuring *per particle* correlations, typically $O(1)$ for all centralities, $\bar{N}$ is the mean multiplicity in the acceptance) for four centrality classes of Au-Au collisions. Those distributions are dominated by 1) a 1D quadrupole component $\propto \cos(2\phi_\Delta)$ conventionally attributed to elliptic flow; 2) a 1D dipole component $\propto \cos(\phi_\Delta)$ associated with transverse momentum conservation for parton scattering and bulk hadronization, and 3) a 2D 'same-side' ($|\phi_\Delta| < \pi/2$) peak, which is the main subject of this analysis. We associate that peak with parton fragmentation to hadrons, albeit for lower-p_t fragments than are usually considered in a conventional jet analysis: minijets.

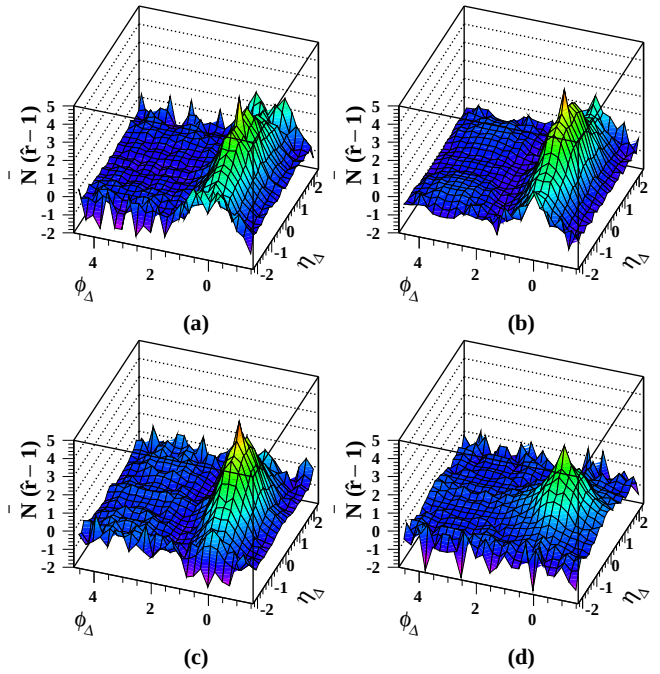

FIG. 2: Same data as in Fig. 1, but η_Δ-independent dipole and quadrupole components on ϕ_Δ (see text) have been subtracted to reveal 'same-side' ($|\phi_\Delta| < \pi/2$) structures which can be associated with minijets.

We expect back-to-back ($\phi_\Delta \sim \pi$) azimuth correlations from momentum conservation in hard parton scattering. However, at low p_t the away-side di-jet structure is broad, and indistinguishable from the dipole $cos(\phi_\Delta)$ component describing momentum conservation in the bulk system. We subtract dipole and quadrupole $cos(2\phi_\Delta)$ components from distributions in Fig. 1 to obtain Fig. 2 by minimizing their residuals on the away side ($|\phi_\Delta| > \pi/2$) and for $|\eta_\Delta| \sim 2$. The same-side 2D peaks in this figure are the main subject of this analysis. We observe that the away-side hemicylinder in Fig. 2 is featureless, even for the most peripheral collisions. If Lund-model strings [21] remained dynamically relevant we would expect in this p_t interval significant correlation structure on the away side of Fig. 2: a prominent gaussian on η_Δ due to local charge conservation as observed in p-p collisions [22, 23]. Lack of such structure suggests that longitudinal strings are *not significant*, even for the most peripheral collisions in this study (Fig. 2d).

The same-side peak isolated by the multipole subtraction varies strongly with centrality, transitioning from nearly symmetric on $(\eta_\Delta, \phi_\Delta)$ for peripheral collisions to dramatically broadened along η_Δ for the more central collisions. The small excess in (0,0) bins is due to conversion-electron pairs. SSC pair cuts reduce the bins nearest (0,0) by 10% or less. 1D projections and model fits on difference variables ϕ_Δ and η_Δ are shown in Fig. 3. Solid dot (open triangle) data symbols correspond to η_Δ (ϕ_Δ) projections.

Statistical errors for joint autocorrelations approximately double as $|\eta_\Delta|$ increases from 0 to 2 because of limited η acceptance, but are uniform on ϕ_Δ because ϕ is periodic. Statistical errors for $\hat{r}$ at $|\eta_\Delta| = 0$ vary from 0.0001 for central collisions to 0.001 for peripheral collisions. Statistical errors for $\bar{N}(\hat{r}-1)$ (~ 0.1) are nearly independent of centrality. Systematic errors were estimated as in [14]. Contamination from photon conversions to $e^{\pm}$ pairs is significant only within the bin defined by $|\eta_\Delta| < 0.1$, $|\phi_\Delta| < 0.1$ which was excluded from model fits. The dominant source of systematic error is non-primary background [15], whose correlation with primary particles is unknown and is estimated by assuming correlations vary from zero to the measured correlation amplitude for primary particles [14]. Total systematic errors for data presented in Fig. 1 are $\pm 7\%$ of signal, but increase to $\pm 8\%$ for $|\eta_\Delta| < 0.5$ and to $\pm 11\%$ for $|\phi_\Delta| < 0.05$. Correlations from resonance (ρ^0, ω) decays were 3% of peaks in Fig. 2 in $|\eta_\Delta| < 0.5$, $|\phi_\Delta| < 2$ [24].

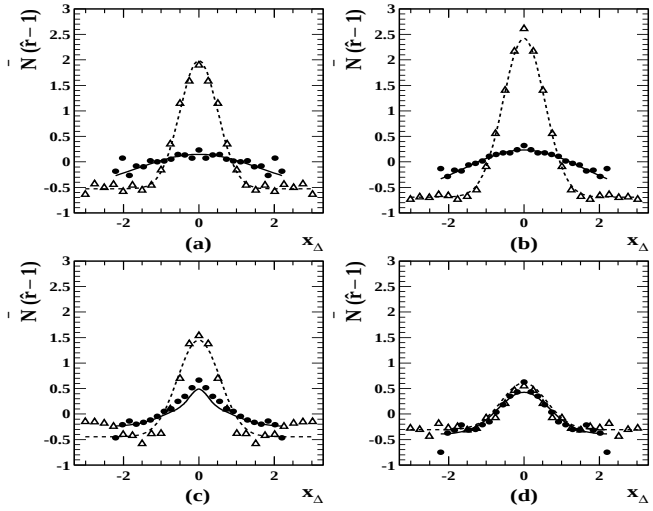

FIG. 3: Projections of 2D CI joint autocorrelations $\bar{N}(\hat{r}-1)$ in Fig. 2 onto difference variables η_Δ (solid dots) and ϕ_Δ (open triangles). Solid (dashed) curves represent corresponding projections of 2D analytical model fits to the data. 2D peaks are substantially reduced in amplitude by 1D projections.

Joint autocorrelations in Fig. 1 (but without factor $\bar{N}$) were fitted with a model function consisting of dipole and quadrupole terms on ϕ_Δ, a 1D gaussian on η_Δ only and a 2D same-side gaussian on $(\eta_\Delta, \phi_\Delta)$, plus constant offset

$$F = A_{\phi_\Delta} \cos(\phi_\Delta) + A_{2\phi_\Delta} \cos(2\,\phi_\Delta) + A_0\, e^{-\left(\frac{\eta_\Delta}{\sqrt{2}\sigma_0}\right)^2} + A_1\, e^{-\left\{\left(\frac{\phi_\Delta}{\sqrt{2}\sigma_{\phi_\Delta}}\right)^2 + \left(\frac{\eta_\Delta}{\sqrt{2}\sigma_{\eta_\Delta}}\right)^2\right\}} + A_2. \quad (2)$$

Best-fit parameters for the model fits shown in Fig. 3 are listed in Table I, including efficiency-correction factor $\mathcal{S}$ [25]. Those fit parameters confirm that with increasing centrality 2D peak structures exhibit 1) strong and non-monotonic amplitude variation, 2) strong η_Δ width increase and 3) significant ϕ_Δ width *reduction*.

TABLE I: Parameters and fitting errors (only) for model fits [Eq. (2)] to joint autocorrelation data in Fig. 1 for centrality bins (a) - (d) (central - peripheral). Total systematic error for efficiency-corrected amplitudes is 11% [25].

centrality	(d)	(c)	(b)	(a)	error[a](%)
$\mathcal{S}$[25]	1.19	1.22	1.25	1.27	8 (syst)
$\bar{N}$	115.5	424.9	790.2	983.0	
$\mathcal{S}\bar{N}A_1$	1.93	3.23	3.72	3.10	5-2
σ_{ϕ_Δ}	0.61	0.55	0.54	0.53	4-2
σ_{η_Δ}	0.58	1.05	1.34	1.36	5-2
$\mathcal{S}\bar{N}A_0$	0.60	0.32	—	—	0.16-0.1[b]
σ_0	1.11	0.24	—	—	28-22
$\mathcal{S}\bar{N}A_2$	-0.67	-0.55	-0.67	-0.58	0[c]
$\mathcal{S}\bar{N}A_{\phi_\Delta}$	-0.31	-0.76	-0.97	-0.74	22-5
$\mathcal{S}\bar{N}A_{2\phi_\Delta}$	1.05	2.72	1.30	0.32	2-17
χ^2/DoF	$\frac{439}{316}$	$\frac{419}{316}$	$\frac{675}{316}$	$\frac{415}{316}$	

[a]Range of fitting errors in percent from peripheral to central.
[b]Magnitude of fitting errors.
[c]Fixed by normalization of $\hat{r}$

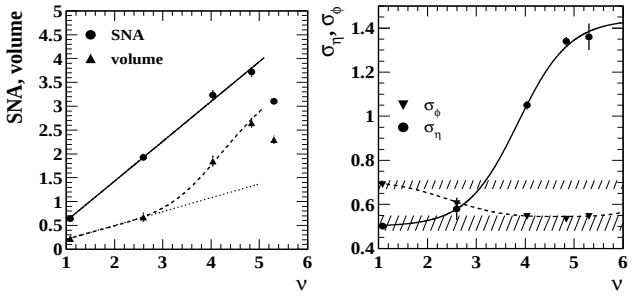

FIG. 4: Left: Fitted amplitudes and volumes for peaks in Fig. 2 plotted on mean participant path length ν [26], from Table I. Right: Fitted widths σ_{η_Δ} (dots) and σ_{ϕ_Δ} (triangles). Hatched regions show p-p values. Curves guide the eye.

Same-side peak amplitudes and widths from model fits are plotted *vs* centrality measure ν in Fig. 4 with values obtained from p-p collisions. Same-side autocorrelations in Fig. 2 differ strongly from those for p-p collisions, where a nearly-symmetric 2D gaussian peak dominates same-side structure with similar widths on η_Δ and ϕ_Δ ($\sim$ 0.5 and 0.7 respectively) [23]. Same-side correlations for peripheral Au-Au collisions (Fig. 2d) are similar to the p-p result. In central Au-Au collisions the two widths of the gaussian peak differ by a factor 2.6. Per-particle amplitude $\mathcal{S}\bar{N}A_1$ for the same-side peak increases nearly linearly with path-length as expected for *independent* binary collisions. However, peak *volume* $\equiv \mathcal{S}\bar{N}A_1\,\sigma_{\eta_\Delta}\,\sigma_{\phi_\Delta}$ ($\propto$ minijet fragment number) has a more complex variation, strongly departing from linear ν scaling (dotted line) above $\nu = 2.5$ (left-panel dashed curve is derived from curves for amplitude and peak widths). The volume excess beyond the linear extrapolation may indicate onset of a strongly dissipative medium in which more fragments with less p_t result from each scattered parton. It is notable that the *amplitude* does not deviate from a linear trend, except for the most central point.

Symmetric same-side angular correlations in p-p collisions, and the peripheral Au-Au result in this study, represent expected *in vacuo* jet fragmentation. We speculate that the mechanism modifying the same-side peak in central Au-Au collisions is strong coupling of *minimum-bias* semi-hard partons (no high-p_t trigger is imposed) to a longitudinally-expanding colored medium developed in the more central Au-Au collisions. Hadron fragments sample the local velocity structure of the pre-hadronic parton-medium coupled system. Growth of the colored medium with collision centrality is then indicated by increased width on η_Δ of the same-side correlation peak.

Hijing [5] same-side angular correlations increase in width by 10% on both η_Δ *and* ϕ_Δ with jet quenching imposed, seriously underpredicting the large width increase on η_Δ and contradicting the width decrease on ϕ_Δ observed in data. The pQCD jet-quenching mechanism in Hijing does not produce an asymmetry on $(\eta_\Delta, \phi_\Delta)$, given the symmetry about the jet thrust axis of its perturbative bremsstrahlung quenching model. Prominent low-p_t string-fragment correlations on η_Δ appear in all Hijing centralities. RQMD [12] CI correlations are essentially featureless except for flow-related correlations on ϕ_Δ.

In conclusion, we have for the first time measured charge-independent joint autocorrelations on difference variables ϕ_Δ *and* η_Δ for Au+Au collisions at $\sqrt{s_{NN}} = 130$ GeV. Low-p_t string-fragment correlations prominent in p-p collisions are not observed for any centrality; longitudinal string degrees of freedom are strongly suppressed even for the most peripheral Au-Au collisions in this study. However, other large-amplitude correlation structures are observed. In addition to azimuth structures associated with elliptic flow and transverse momentum conservation we observe a near-side peak structure varying from a symmetric shape on $(\eta_\Delta, \phi_\Delta)$ in peripheral collisions to a highly elongated shape on η_Δ in central collisions. That deformation trend, observed in this first jet analysis with *low-p_t* hadrons, can be interpreted as a transition from *in vacuo* jet fragmentation in p-p and peripheral Au-Au collisions to coupling of minimum-bias partons to a longitudinally-expanding colored medium in the more central collisions as part of a dissipation process. The concept of parton energy loss in heavy ion collisions [5, 8] is thereby extended to strongly non-perturbative aspects.

We thank the RHIC Operations Group and RCF at BNL, and the NERSC Center at LBNL for their support. This work was supported in part by the HENP Divisions of the Office of Science of the U.S. DOE; the U.S. NSF; the BMBF of Germany; IN2P3, RA, RPL, and EMN of France; EPSRC of the United Kingdom; FAPESP of Brazil; the Russian Ministry of Science and Technology; the Ministry of Education and the NNSFC of China; Grant Agency of the Czech Republic, FOM and UU of the Netherlands, DAE, DST, and CSIR of the Government of India; Swiss NSF; and the Polish State Committee for Scientific Research.

[1] R. Stock, Nucl. Phys. **A661**, 282 (1999); H. Heiselberg, Phys. Rep. **351**, 161 (2001).
[2] A. Dumitru, R. Pisarski, Phys. Lett. **B504**, 282 (2001).
[3] L. M. Bettencourt, K. Rajagopal and J. V. Steele, Nucl. Phys. **A693**, 825 (2001).
[4] M. Gaździcki, A. Leonidov, G. Roland, Eur. Phys. J. **C6**, 365 (1999).
[5] X.N. Wang, M. Gyulassy, Phys. Rev. D **44**, 3501 (1991).
[6] Q. Liu and T. A. Trainor, Phys. Lett. **B567**, 184 (2003).
[7] C. Adler *et al.*, Phys. Rev. Lett. **90**, 082302 (2003).
[8] N. Armesto, C. A. Salgado and U. A. Wiedemann, hep-ph/0405301.
[9] R. Hwa and C. Yang, Phys. Rev. C **66**, 025205 (2002).
[10] An autocorrelation is a projection by averaging of a distribution on (x_1, x_2) onto difference variable $x_1 - x_2$.
[11] H. R. Schmidt and J. Schukraft, J. Phys. G: Nucl. Part. Phys. **19**, 1705 (1993).
[12] H. Sorge, H. Stöcker, W. Greiner, Nucl. Phys. **A498**, 567c (1989); Ann. Phys. (N.Y.) **192**, 266 (1989).
[13] K. H. Ackermann *et al.*, Nucl. Instrum. Meth. A **499**, 624 (2003); see other STAR papers in volume A**499**.
[14] J. Adams *et al.* (STAR Collaboration), nucl-ex/0308033.
[15] C. Adler *et al.*, Phys. Rev. Lett. **87**, 112303 (2001); *ibid.* **89**, 202301 (2002).
[16] Track cuts required minimum track separations 5, 12 and 20 cm at radii 50, 127 and 200 cm from the TPC axis. Crossing pairs with separations less than 10 cm (z) and 30 cm (azimuth) at mid-radius were also excluded.
[17] C. Adler *et al.* Phys. Rev. Lett. **87**, 082301 (2001).
[18] Centrality classes d) - a) for 300k events were defined by N/N_0 [19] cuts at > 0.03, 0.21, 0.56 and > 0.79.
[19] N_0, the half-max point at the end of the minimum-bias distribution plotted as $d\sigma/dN_{ch}^{1/4}$, is an estimator on multiplicity N for the maximum number of participant nucleons; $N/N_0 \simeq N_{part}/N_{part,max}$ within 4%.
[20] J. Adams *et al.* (STAR Collaboration), submitted to PRL, eprint nucl-ex/0406035.
[21] B. Andersson, G. Gustafson, G. Ingelman and T. Sjöstrand, Phys. Rep. **97**, 31 (1983).
[22] J. Whitmore, Phys. Rep. **27**, 187 (1976).
[23] R. J. Porter and T. A. Trainor (STAR Collaboration), eprint hep-ph/0406330.
[24] R. Ray and R. Longacre, nucl-ex/0008009, unpublished.
[25] Extrapolation factors $\mathcal{S}$ for $\bar{N}(\hat{r}-1)$ [14] correct for contamination and inefficiency [15]. Systematic error in $\mathcal{S}$ was estimated to be $\pm 8\%$. Total systematic error for extrapolated quantities in Table I was 11%.
[26] Quantity $\nu \equiv (N_{part}/2)^{1/3} \simeq 5.5(N/N_0)^{1/3}$ for Au (N_{part} is participant number) estimates mean participant path length in number of encountered nucleons.